Exchange coupling of ferromagnetic films across metallic and semiconducting interlayers

D E Bürgler[1]**, M Buchmeier**[1]**, S Cramm**[1]**, S Eisebitt**[2]**, R R Gareev**[1]**,
P Grünberg**[1,4]**, C L Jia**[1]**, L L Pohlmann**[1]**, R Schreiber**[1]**, M Siegel**[3]**,
Y L Qin**[1] **and A Zimina**[2]

[1] Institut für Festkörperforschung, Forschungszentrum Jülich GmbH, Germany
[2] BESSY GmbH, Berlin, Germany
[3] Institut für Schichten und Grenzflächen, Forschungszentrum Jülich GmbH, Germany

E-mail: P.Gruenberg@fz-juelich.de

Abstract

Recent results obtained in our laboratories on interlayer exchange coupling
of Fe films across interlayers of iron silicides, $Fe_{1-x}Si_x$ with $x = 0.5$–1, are
reviewed. Samples are prepared by molecular beam epitaxy and characterized
by means of low-energy electron diffraction and cross-sectional transmission
electron microscopy. Coupling across interlayers of iron silicide with $x \approx 0.5$ is
found to be oscillatory with a strength of the order of 1 mJ m^{-2}, and across well
ordered Si interlayers (nominally $x = 1$) the coupling is exponentially decaying.
In the latter case the maximum coupling turns out to be surprisingly strong
(>6 mJ m^{-2}), in particular considering the fact that the electrical resistivity is
found to be large. Current–voltage curves for currents across the interlayers
are characteristic of electron tunnelling. Soft-x-ray emission and near-edge
x-ray absorption spectroscopy further support a semiconducting nature for the
nominally pure Si interlayers.

1. Introduction

Interlayer exchange coupling (IEC) across metallic interlayers has been extensively
investigated, and it is now well established that IEC generally displays a damped oscillation
between the ferromagnetic and antiferromagnetic states as a function of the interlayer thickness.
The oscillation period is given by certain features, called *stationary vectors*, at the Fermi surface
of the interlayer material [1, 2]. Theoretically, it was shown that this oscillatory coupling is
due to the formation of standing electron waves in the interlayer, which result from spin-
dependent electron interface reflectivity [3, 4]. On replacing the electron wave with a light
wave, there is a certain analogy to an optical Fabry–Perot interferometer. Therefore, this

[4] Author to whom any correspondence should be addressed.

model is sometimes called the *Fabry–Perot model* of IEC. For insulating and semiconducting interlayers, there are only evanescent waves decaying away from the interfaces with the metallic, magnetic layers. Accordingly, from theory, the exchange coupling is expected to be exponentially decaying as the thickness of the interlayer increases [3, 4]. For good insulators (e.g. SiO_2 and Al_2O_3), IEC has never been observed experimentally—supposedly because it is too weak. Therefore for semiconducting interlayers, one would expect it to be weaker than in metals, but possibly observable. Indeed, Toscano *et al* [5] found weak oscillatory coupling across amorphous Si interlayers, whereas Fullerton *et al* [6] reported somewhat stronger, but non-oscillatory coupling with increasing strength for increasing temperature. After some controversial discussion between various groups, de Vries *et al* [7] suggested that in the Fe/Si/Fe structures investigated the Si had in reality turned into a metallic silicide of composition $Si_{0.5}Fe_{0.5}$ due to Fe diffusion, and that the coupling across the silicide was exponentially decaying. Even in metals there can be certain directions in the Brillouin zone with gaps at the Fermi level, which could explain the observed exponential decay [3, 4].

However, the fact that these results were obtained on samples where the Fe had diffused into the Si in an uncontrolled way seemed unsatisfactory. We therefore decided to repeat these experiments with samples where the Si is doped with various amounts of Fe in a controlled way during the deposition, namely by co-deposition of Fe and Si from two independent e-beam sources. Briefly, for sufficiently large Fe content in the interlayer, we find oscillatory behaviour of the coupling [8], which transforms into an exponential decay upon increasing the Si content [9]. At the same time, surprisingly, the maximum antiferromagnetic coupling strength becomes much stronger than for most cases with metallic interlayers.

Therefore, we pay particular attention here to the electronic nature of the interlayer. Both transport measurements for currents perpendicular to the film plane (CPP geometry) as well as electronic structure measurements by soft-x-ray emission (SXE) spectroscopy combined with near-edge x-ray absorption spectroscopy (NEXAFS) support a semiconducting nature for our nominally pure Si interlayers. In section 2 we describe the most important features of the sample preparation and characterization and give some detail on how we determine the coupling strength. In section 3 we report on our recent results on IEC in Fe/Si/Fe and $Fe/Fe_{1-x}Si_x/Fe$ systems and present transport measurements as well as SXE/NEXAFS data to provide some further evidence for the semiconducting nature of the nominally pure Si in our Fe/Si/Fe structures.

2. Experimental details

2.1. Sample preparation and characterization

$Fe/Fe_{1-x}Si_x/Fe$ trilayers ($x = 0.5–1$) are prepared by molecular beam epitaxy (MBE) under ultrahigh-vacuum (UHV) conditions (base pressure $< 10^{-10}$ mbar) onto monocrystalline, 150 nm thick Ag(001) buffer layers grown at 375 K on UHV-annealed GaAs(001) wafers covered with a 1 nm thick Fe seed layer (figure 1). By moving a shutter in front of the substrate during the deposition of the interlayer, wedge-shaped interlayers can be produced, where the term *wedge* refers to an increase of the interlayer thickness t from 0 to approximately 5 nm over a lateral distance of about 1 cm. The $Fe_{1-x}Si_x$ interlayers are prepared by co-deposition of Fe and Si from separate crucibles with well controlled rates. The composition parameter x can thus be determined from the rates (i.e. the atomic fluxes of Fe and Si), and also from Auger spectroscopy data obtained after the deposition of the interlayer. There is perfect agreement between the calculated and measured compositions.

The samples are also characterized by means of low-energy electron diffraction (LEED) patterns taken at various stages of the preparation. Figure 2(a) shows a pattern from the bottom
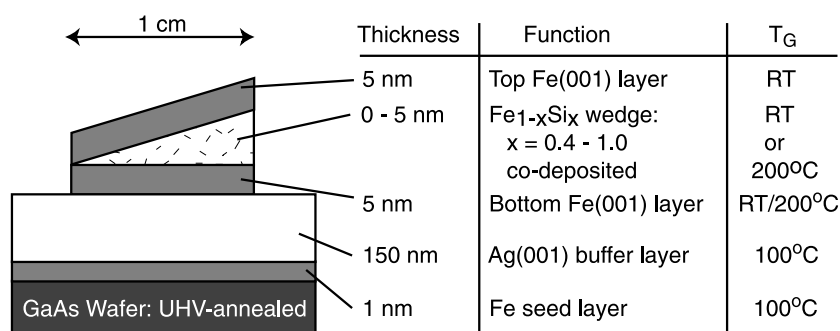
Thickness	Function	T_G
5 nm	Top Fe(001) layer	RT
0 - 5 nm	Fe$_{1-x}$Si$_x$ wedge: x = 0.4 - 1.0 co-deposited	RT or 200°C
5 nm	Bottom Fe(001) layer	RT/200°C
150 nm	Ag(001) buffer layer	100°C
1 nm	Fe seed layer	100°C

Figure 1. Sample structure (left), thickness, function, and growth temperature T_G of the layers (right). $T_G = $ RT/200 °C for the bottom Fe layer means that growth starts at RT and T_G is increased to 200 °C after deposition of four monolayers in order to minimize Ag segregation. Fe$_{0.5}$Si$_{0.5}$ interlayers were grown at 200 °C, whereas Si-rich interlayers ($x > 0.5$) were grown at RT. Real wedges are much flatter than indicated in this figure.
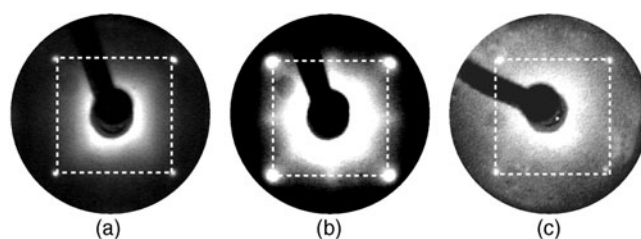

Figure 2. LEED patterns taken at 55 eV electron energy. (a) A 5 nm thick, bottom Fe(001) layer; (b) a 0.5 nm thick Fe$_{0.5}$Si$_{0.5}$ interlayer grown at 200 °C on a bottom Fe layer; and (c) a 0.5 nm thick nominally pure Si interlayer grown at RT on a bottom Fe layer.

Fe film. It is representative of the (100) plane of the bcc structure of Fe. Figure 2(b) displays a LEED pattern from the surface of a 0.5 nm thick Fe$_{0.5}$Si$_{0.5}$ interlayer grown at 200 °C on a bottom Fe layer. One can see additional spots sited at the edges of the dashed square, which is identically superimposed in all three images. These spots indicate a doubling of the unit-cell size, which is expected when every other Fe atom along [100] directions is replaced by Si. Hence, the Fe$_{0.5}$Si$_{0.5}$ interlayer displays a well defined, pseudomorphic structure. In figure 2(c), we see the diffraction pattern from a nominally pure (i.e. deposition conditions for $x = 1.0$), 0.5 nm thick Si interlayer grown at room temperature (RT), which is practically identical to the pattern from the Fe film (figure 2(a)) on which it was grown. Hence, the growth of a thin Si layer on Fe(001) is pseudomorphic.

Figure 3 displays a cross-sectional transmission electron microscopy (TEM) picture of an Fe/Si/Fe structure with a nominally pure, 5 nm thick Si interlayer. The Fe/Si/Fe trilayer is covered by additional Si for protection. Both the Fe/Si and the Si/Fe interfaces of the Fe/Si/Fe structure are sharp, excluding the possibility of appreciable interdiffusion. Only the topmost Fe/Si interface between the top Fe layer and the thick Si protection layer is diffuse, but this is not of importance, because the effect of this interface on the coupling can be neglected due to the relatively thick Fe top layer.
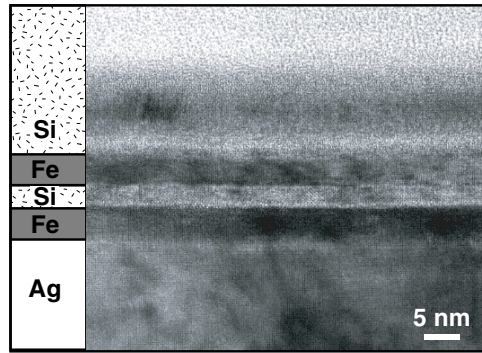
Figure 3. A cross-sectional TEM image of an Fe/Si/Fe trilayer covered with a thick Si protection layer. The Si interlayer appears as a light grey band with sharp boundaries towards the adjacent Fe layers.

2.2. Determination of the coupling type and strength

IEC of ferromagnetic 3d metals across interlayers is conventionally described by the phenomenological areal energy density σ_{IEC}:

$$\sigma_{IEC} = -J_1 \cos(\vartheta) - J_2 \cos^2(\vartheta). \tag{1}$$

Here, ϑ is the angle between the magnetizations of the films on either side of the spacer layer. The standard method for the determination of J_1 is the measurement of remagnetization curves, mostly by means of the magneto-optic Kerr effect (MOKE hysteresis). The parameters J_1 and J_2 describe the type and the strength of the coupling. If the term with J_1 dominates, then from the minima of equation (1), the coupling is ferromagnetic (antiferromagnetic) for positive (negative) J_1. If the term with J_2 dominates and is negative, we obtain 90° coupling. The first term of equation (1) is often called bilinear coupling and the second biquadratic coupling. Biquadratic coupling is thought to be mainly due to interface roughness and will not be considered further here. Bilinear coupling, on which we concentrate in the following, describes IEC. For antiferromagnetic IEC, the methods employing remagnetization curves are straightforward, but in the case of ferromagnetic coupling, samples with *spin engineering layers* [10] need to be prepared. In contrast, if spin-wave properties are exploited [11–13], then samples of the same type can be used for ferromagnetic as well as antiferromagnetic coupling. This is particularly important for samples with wedge interlayers, because ferromagnetic- and antiferromagnetic-type coupling can occur at different interlayer thicknesses of the same sample. Furthermore, the spin-wave method works also for vanishing field (a small field is mostly applied to provide assurance of the orientation of the parallel-or antiparallel-aligned magnetizations). For the results discussed in the following, the MOKE technique and the spin-wave method (Brillouin light scattering, BLS) have been employed as appropriate.

3. IEC across $Fe_{1-x}Si_x$ (x = 0.5–1) interlayers

Figure 4 shows the switching fields, which are a measure for the total coupling strength, as a function of the spacer thickness t for the samples with the nominally 1:1 Fe–Si composition deposited at 200 °C and measured at 20 and 300 K. We observe an oscillatory behaviour of the coupling versus spacer thickness over the whole temperature range. Two distinct regions with clear coupling maxima are found near $t = 18$ and 39 Å. Note that we give here all spacer
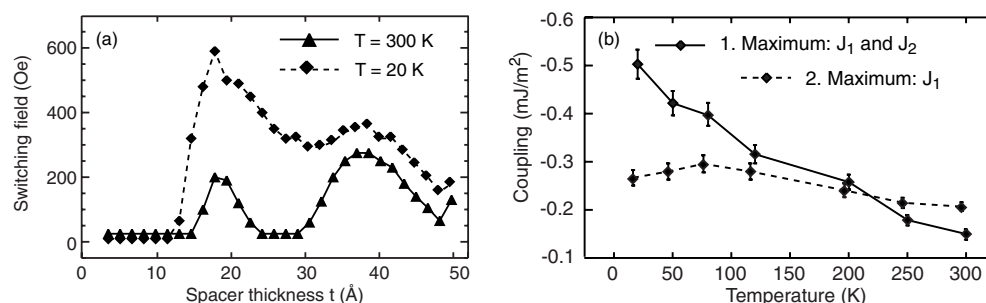
Figure 4. (a) Switching fields determined from the MOKE as a measure of the total coupling versus the spacer thickness of a wedge-type Fe(5 nm)/Fe$_{0.5}$Si$_{0.5}$(t)/Fe(5 nm) trilayer, measured at 300 K and 20 K. (b) Total coupling strengths at the first and second coupling maxima, as a function of temperature. The different behaviour at low temperatures arises from the fact that J_1 and J_2 have different temperature dependences. J_1 dominates in the second maximum, whereas there is a significant contribution from J_2 in the first maximum.

thicknesses as the sum of the quartz monitor readings for Fe and Si. We do not take into account the volume contraction associated with the formation of a silicide, which may be rather large, e.g. 33% for Fe$_{0.5}$Si$_{0.5}$ [7]. We note that the data in figure 4(a) represent the first observation of clear oscillatory interlayer coupling across FeSi spacers. The position of the first peak (about 12 Å after volume contraction) matches the results of de Vries *et al* [7], but the second peak contradicts their exponential decay of the coupling. We relate this discrepancy to

 (i) the more homogeneous spacer of our samples and
(ii) the larger epitaxial spacer thickness range accessible in our experiments.

Both advantages arise from the preparation of the FeSi spacer by co-evaporation instead of interdiffusion. A mechanism for how structural disorder in a metallic spacer can lead to an exponential thickness dependence of RKKY-type interlayer coupling is described in [14]. Obviously, only the fact that the thickness of the FeSi spacer is not limited to values smaller than 30 Å (20 Å when the volume contraction is taken into account)—as is the case in [7]—allows one to observe the oscillatory behaviour.

The temperature dependence of the bilinear coupling strength for metallic and insulating spacers can be described by the quantum interference model formulated by Bruno [3]. Oscillations and an increase of the coupling strength upon cooling with saturation at low temperatures are found for metallic spacers. In contrast, for insulating spacers the coupling strength is expected to decay exponentially with spacer thickness and to decrease with decreasing temperature. We emphasize that below 80 K the coupling is also of metallic type, because we observe oscillatory coupling behaviour in figure 4 down to 20 K. For the interlayers with the nominal 1:1 Fe–Si composition, the coupling strength increases with decreasing temperature—at least down to 80 K—but it is always less than 1 mJ m^{-2}. Hence, the temperature dependence, the oscillatory behaviour, and the order of magnitude of the coupling strength all imply that the coupling across ordered FeSi can be understood in terms of the conventional models for interlayer coupling across metallic spacer layers without the need to claim a new type of coupling for this specific material.

The effect of reducing the Fe content in our Fe$_{1-x}$Si$_x$ interlayers on the coupling is displayed in figure 5, which shows the dependence of J_1 on t for interlayers with different nominal Si contents as quoted. The most obvious feature is the drastic increase of the coupling by almost one order of magnitude when the nominal Si content x is increased from 0.5 to 1.0.
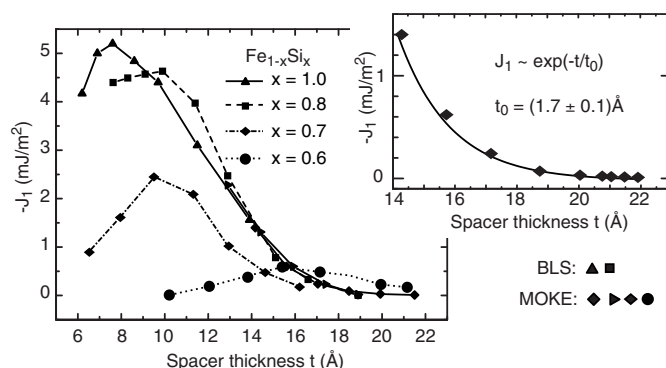
Figure 5. J_1 versus spacer thickness t for Fe(5 nm)/Fe$_{1-x}$Si$_x$(t)/Fe(5 nm) trilayers with spacers of different nominal Si content $x = 0.6, 0.7, 0.8$, and 1.0. The coupling strengths are derived from BLS and MOKE experiments as indicated by the various symbols. Inset: exponential decay of the coupling with spacer thickness t for a nominally pure Si spacer layer.

The coupling strength J_1 is larger than 5 mJ m^{-2} for a nominally pure Si spacer, representing the largest value ever reported for the Fe/Si/Fe system. For the nominally pure Si spacer and sufficiently large t, where J_1 prevails, J_1 decreases exponentially with spacer thickness. The decay length is $t_0 \approx 1.7$ Å (inset of figure 5). The figure reveals also the dependence of the thickness t_{max} of the interlayer, where the maximum coupling occurs, on the nominal Si content x. For an Si-rich spacer, t_{max} is near 10 Å and decreases to 7.7 ± 0.3 Å for $x = 1.0$. The decrease of the coupling strength at small thicknesses, $t < t_{max}$, is very likely related to the presence of ferromagnetic coupling due to pinholes [7]. Both observations—the increase of the maximum coupling strength and the decrease of t_{max} with x—can be understood on the basis of exponentially attenuated coupling disturbed by the existence of ferromagnetic bridges, the influence of which is reduced when the Fe content in the spacer is reduced. The same picture also explains the enhancement of the coupling strength in excess of 8 mJ m^{-2} when a thin boundary layer is introduced at the bottom Fe/Si interface [15], which presumably further reduces the interdiffusion and the formation of pinholes.

The coupling strength of more than 5 mJ m^{-2} for a nominally pure Si spacer is very surprising, as one would expect it to be weaker than across metallic spacers, where values around 1 mJ m^{-2} are more typical. For this reason, we have further investigated the electronic nature of the interlayer by means of transport measurements for currents perpendicular to the film plane across lithographically defined, micron-sized contacts (see the inset of figure 6). The current–voltage (I–V) characteristics of a contact with an area of 22 μm^2 are displayed in figure 6. The resistivity determined from the slope at zero bias (dotted curve) is $>10^6$ $\mu\Omega$ cm, i.e. it is more than 10^5 times the resistivity of Fe. Furthermore, the measured I–V characteristic is non-linear, also suggesting an insulating or semiconducting material rather than a conducting one. The I–V curve can be fitted (dashed curve) assuming that the electrical transport is due to tunnelling. The associated tunnelling barrier height is evaluated by a Brinkman fit to be $\phi = 0.35$ eV.

Further information on the electronic structure of the nominally pure Si interlayer was obtained from preliminary SXE and absorption experiments performed at BESSY. In contrast to the TEM sample of figure 3, the Si interlayer thickness was only of the order of 1 nm and the trilayer was not covered by Si. In figure 7, spectra recorded for the thin and embedded Si interlayer are compared to spectra of a bulk Si wafer. The observed intensities are proportional
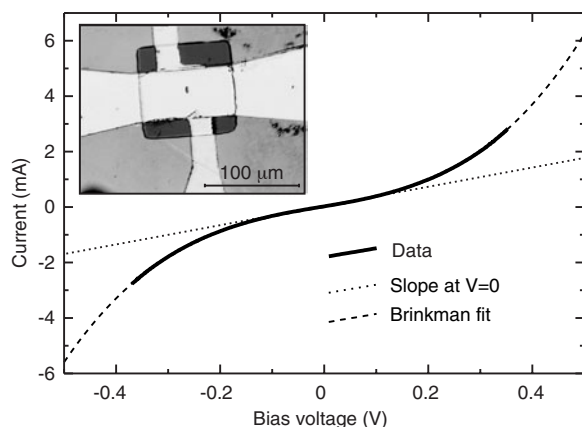
Figure 6. I–V characteristics of a Fe/Si/Fe contact with an area of 22 μm^2. The slope of the dotted curve yields the resistivity at zero bias, and the dashed curve is a Brinkman fit to the data. The inset shows a photograph of a smaller contact (the dark spot in the centre of the image) with the typical crossed electrodes used for four-probe measurements and the square-shaped insulating layer.

to the density of Si s- and d-type electronic states. The position of the Si L$_{2,3}$ edge at about 99 eV corresponds to the Fermi level. The SXE spectrum to the left shows the density of occupied states, and the NEXAFS spectrum to the right the density of unoccupied states. The spectrum of the occupied states indicates that iron silicides are present, possibly in addition to pure Si. The observed density of states can fit a range of stable phases from Fe$_3$Si to FeSi$_2$ [16]. In the present context, we emphasize that we observe a gap at the Fermi energy in both the Si and the Fe/Si/Fe case, supporting a semiconducting nature for the interlayer. More detailed experiments with samples of different spacer compositions and thicknesses are under way, intended to establish, for instance, the correlation between the strong coupling and the presence of a gap.

4. Conclusions

We conclude that the coupling strength of Fe/Fe$_{1-x}$Si$_x$/Fe trilayers increases strongly with increasing nominal Si content x in the spacer layer. We relate the very strong exchange coupling and its exponential decay for nominally pure Si spacers to the growth of semiconducting layers with a high resistivity. We believe that, with increasing x, antiferromagnetic interlayer coupling becomes more dominant compared to the ferromagnetic coupling across pinholes. Therefore, the coupling maximum also shifts to smaller spacer thicknesses, and the strength increases accordingly, due to the exponential increase of J_1 for decreasing t. The new results presented here and our previous results for metallic Fe$_{0.5}$Si$_{0.5}$ spacers [8] allow us to exclude the possibility of diffusive formation of metallic iron silicide spacers being the reason for the observed strong coupling.

A theoretical explanation for the strong coupling and its dependence on the nominal Si content x is lacking at present. Theoretical modellings—including *ab initio* calculations—of pseudomorphic Fe/Fe$_{1-x}$Si$_x$/Fe(100) structures are highly desirable in order to provide a deeper understanding of their coupling and transport properties.
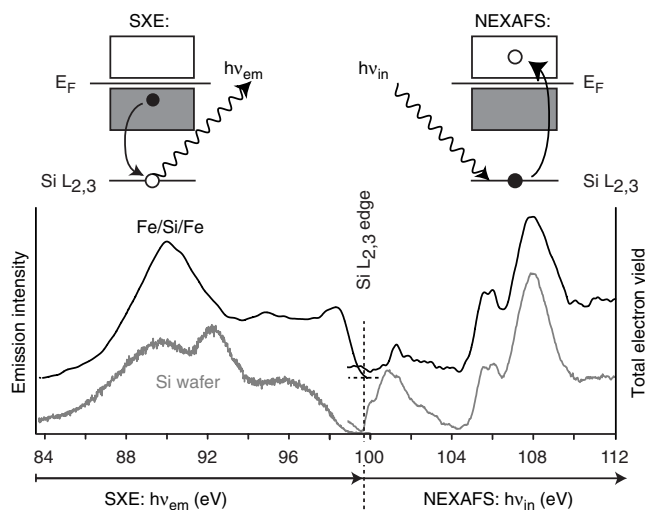
Figure 7. Combined SXE and NEXAFS Si L$_{2,3}$ spectra of an Fe/Si/Fe trilayer (black) compared with spectra of an Si wafer (grey). The curves are vertically offset for clarity, and the zero line for the Fe/Si/Fe spectra is indicated by the horizontal dashed line. SXE (left part) is excited with 130 eV photons, and the NEXAFS spectrum (right part) is measured in total-electron-yield mode. The position of the Si L$_{2,3}$ edge at about 99 eV corresponds to the Fermi level and separates the occupied (left) and unoccupied (right) states.

Acknowledgment

References

[1] Bürgler D E, Grünberg P, Demokritov S O and Johnson M T 2001 *Handbook of Magnetic Materials* vol 13, ed K H J Buschow (Amsterdam: Elsevier) pp 1–85
[2] Grünberg P A and Pierce D T 2001 *Encyclopedia of Materials: Science and Technology* (Amsterdam: Elsevier) pp 5883–8
[3] Bruno P 1995 *Phys. Rev.* B **52** 411
[4] Stiles M D 1999 *J. Magn. Magn. Mater.* **200** 322
[5] Toscano S, Briner B, Hopster H and Landolt M 1992 *J. Magn. Magn. Mater.* **114** L6
[6] Fullerton E E, Mattson J E, Lee S R, Sowers C H, Huang Y Y, Felcher G, Bader S D and Parker F T 1992 *J. Magn. Magn. Mater.* **117** L301
[7] de Vries J J, Kohlhepp J, den Broeder F J A, Coehoorn R, Jungblut R, Reinders A and de Jonge W J M 1997 *Phys. Rev. Lett.* **78** 3023
[8] Gareev R R, Bürgler D E, Buchmeier M, Olligs D, Schreiber R and Grünberg P 2001 *Phys. Rev. Lett.* **87** 157202
[9] Gareev R R, Bürgler D E, Buchmeier M, Schreiber R and Grünberg P 2002 *J. Magn. Magn. Mater.* **240** 237
[10] Parkin S S P 1991 *Phys. Rev. Lett.* **67** 3598
[11] Grünberg P 1989 *Light Scattering in Solids (Springer Topics in Applied Physics vol 66)* ed M Cardona and G Güntherodt (New York: Springer) pp 303–35
[12] Rezende S M, Chesman C, Lucena M A, Azevedo A and de Aguiar F M 1998 *J. Appl. Phys.* **84** 958
[13] Buchmeier M, Kuanr B K, Gareev R R, Bürgler D E and Grünberg P 2002 *Phys. Rev.* B submitted
[14] Bürgler D E, Schaller D M, Schmidt C M, Meisinger F, Kroha J, McCord J, Hubert A and Güntherodt H-J 1998 *Phys. Rev. Lett.* **80** 4983
[15] Gareev R R, Bürgler D E, Buchmeier M, Schreiber R and Grünberg P 2002 *Appl. Phys. Lett.* **81** 1264
[16] Jia J J, Callcott T A, O'Brien W L, Dong Q Y, Mueller D R, Ederer D L, Tan Z and Budnick J I 1992 *Phys. Rev.* B **46** 9446